Surface layer of $SrRuO_3$ epitaxial thin films under oxidizing and reducing conditions

M. Mlynarczyk, K. Szot, A. Petraru, U. Poppe, U. Breuer, R. Waser, and K. Tomala

---

Surface layer of SrRuO$_3$ epitaxial thin films under oxidizing and reducing conditions

M. Mlynarczyk,[a)] K. Szot, A. Petraru, U. Poppe, U. Breuer, and R. Waser
*Institut für Festkörperforschung, Forschungszentrum Jülich, 52425 Jülich, Germany
and Center of Nanoelectronic Systems for Information Technology, Forschungszentrum Jülich,
52425 Jülich, Germany*

K. Tomala
M. Smoluchowski Institute of Physics, Jagiellonian University, Reymonta 4, 30-059 Kraków, Poland

Imperfect stoichiometry and heterogeneity of a surface layer of SrRuO$_3$ epitaxial thin films, grown on SrTiO$_3$ substrates, are presented with the help of various methods. Rutherford backscattering spectroscopy, x-ray photoemission spectroscopy (XPS), and time of flight secondary ion mass spectrometry are used to obtain information about the stoichiometry and uniformity of the SrRuO$_3$ structure. The temperature of chemical decomposition is first determined for polycrystalline samples under different conditions using thermogravimetry analysis. Then the determined values are used for thin film annealings in high and low oxygen pressure ambients, namely, air, vacuum, and hydrogen. The surface deterioration of the thin film together with changes in its electronic structure is investigated. O1s and Sr3d core lines measured by XPS for as-made samples obviously consist of multiple components indicating different chemical surroundings of atoms. Thanks to different incident beam angle measurements it is possible to distinguish between interior and surface components. Valence band spectra of the interior of the film are consistent with theoretical calculations. After annealing, the ratio of the different components changes drastically. Stoichiometry near the surface changes, mostly due to ruthenium loss (RuO$_X$) or a segregation process. The width and position of the Ru3p line for as-made samples suggest a mixed oxidation state from metallic to fully oxidized. Long annealing in hydrogen or vacuum ambient leads to a complete reduction of ruthenium to the metallic state. Local conductivity atomic force microscopy scans reveal the presence of nonconductive adsorbates incorporated in the surface region of the film. Charge transport in these measurements shows a tunneling character. Scanning tunneling microscopy scans show some loose and mobile adsorbates on the surface, likely containing hydroxyls. These results suggest that an adequate description of a SrRuO$_3$ thin film should take into account imperfections and high reactivity of its surface region. © *2007 American Institute of Physics*. [DOI: 10.1063/1.2408382]

I. INTRODUCTION

In the course of research done within the decade on the perovskite compound family, SrRuO$_3$ thin films have attained the status of a nearly perfect material to be applied both in basic research and in technological designs. Basic studies covered a wide range of properties of the material itself,[1,2] including such phenomena as quantum oscillations in electrical resistivity,[3] Hall effect sign reversal,[4] or magnetic anisotropy.[5] Other studies concerned changes induced by substitution of *A*-site element (Sr) with Ca, La, or Na; by substitution of *B*-site element (Ru) with Ti, Fe, Co, Mn, or Sn;[6–10] and also by introduction of oxygen deficiency[11] or ruthenium excess.[12] For instance a certain concentration of titanium turns the film into a paramagnetic insulator,[13] calcium doping suppresses ferromagnetism, while the material remains conductive,[14] and oxygen vacancies are reflected in the increase of resistivity of the film.[11] The metallic behavior of SrRuO$_3$ and its pseudocubic lattice constant, which is similar to many different perovskite related materials, allow a large area of applications. SrRuO$_3$ is not only a standard bottom electrode for the (Pb,La)(Zr,Ti,Nb)O$_3$ and (Ba,Sr)TiO$_3$ families of ferroelectric capacitors[15,16] but it is also a common metal layer in SrRuO$_3$/YBa$_2$Cu$_3$O$_7$ Josephson junctions,[17] SrRuO$_3$/Sr$_2$YRuO$_6$ magnetic tunnel junctions,[18] and others.

Naturally one may be inclined to characterize SrRuO$_3$ thin film in general as a pseudocubic *AB*O$_3$ perovskite of a uniform, bulklike structure and perfect stoichiometry, deposited from a stoichiometric target. Its extreme thermal, chemical, and electrical stability[19–21] would allow deposition, cleaning, and utilization using any standard procedure, under virtually any possible conditions. In fact it is well known that under oxidizing conditions ruthenium forms RuO$_4$ oxide which is volatile. To compensate possible Ru loss commercially available targets usually contain significant excess of ruthenium. Because *B*-site ions in *AB*O$_3$ perovskite structure have a low solubility limit,[22] separate RuO$_2$ domains are observed. Volatility of ruthenium oxides may produce some nonstoichiometry at the surface layer. Even for a model per-

a)Electronic mail: wind_mill@poczta.onet.pl

ovskite material, such as $SrTiO_3$, there exist several, well described mechanisms which affect stoichiometry near the surface, such as segregation of SrO under oxidizing or reducing conditions.[23] In the case of $SrRuO_3$ their influence will coexist with possible sublimation of Ru compounds, making its surface layer very interesting to investigate.

In this work deviation from stoichiometry, such as Ru deficit at both interface and surface, was observed using Rutherford backscattering spectroscopy (RBS), x-ray photoemission spectroscopy (XPS), and time of flight secondary ion mass spectrometry (ToF SIMS). Nevertheless for legibility of this report the structure of studied thin films is being referred to as $SrRuO_3$.

Under different conditions there exist several reports stating that $SrRuO_3$ is highly reactive in atmospheres containing hydrogen at temperatures as low as 200 °C,[24] that it decomposes during vacuum annealing close to a temperature of 600 °C,[24] and that structural changes may appear when different layers are deposited on top of $SrRuO_3$.[19] Therefore a stability of the $SrRuO_3$ thin films is rather limited. The films are stable when a deposition or a treatment proceeds in oxygen containing ambience within certain limits of an oxygen partial pressure and temperature. This work points out some aspects of defect chemistry, emphasizing the role of the morphology and electronic structure imperfection of the surface layer of $SrRuO_3$ thin films, as an important feature to understand properties of $SrRuO_3$ thin films and $SrRuO_3$ containing multilayer structures.

The $SrRuO_3$ thin films have been grown by various techniques. Mostly pulsed laser deposition (PLD), using XeCl or KrF excimer laser, has been performed at deposition temperatures varying from 350 to 810 °C and oxygen pressures in the range of 0.03–0.5 mbar.[11,25] Usually preparation conditions were optimized to obtain the lowest resistivity and a flat surface. The best films, with a room temperature resistivity of about 150–300 $\mu\Omega$ cm, root mean square (rms) roughness about 0.1 nm, and rocking curves with full width at half maximum (FWHM) lower than 0.1°, have been produced at temperatures of 640–800 °C and oxygen pressures of 0.1–0.4 mbar.[11,26] Several other procedures, such as 90° off-axis sputtering[27] in temperature and pressure ranges of 300–680 °C and 0.03–0.1 mbar, respectively, techniques requiring extremely low oxygen pressures (10^{-6}–10^{-3} mbar) such as magnetron sputtering,[28] ion beam sputtering,[12] or molecular beam epitaxy,[29] but also high pressure sputtering,[30] metal organic chemical vapor deposition,[31] or spin coating,[32] have been successfully applied. Most of them give results comparable to PLD. Generally $SrTiO_3$ substrates have been utilized, because of the small lattice mismatch. Also $LaAlO_3$ and MgO substrates were used whenever a strain resulting from a large lattice parameter misfit was desired.[33]

II. EXPERIMENT

The $SrRuO_3$ thin films were grown on exact (001) $SrTiO_3$ substrates (tolerance <0.5°) by dc high pressure on-axis sputtering. The substrates without any special treatment displayed a smooth surface with a periodic step terrace struc-
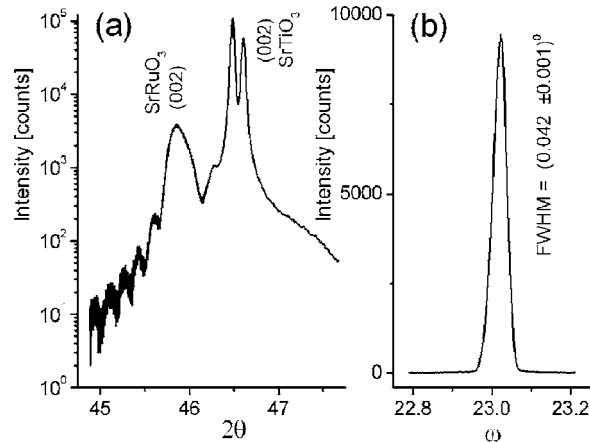

FIG. 1. X-ray θ-2θ scan (a) and ω-rocking curve (b) of (002) peak of $SrRuO_3$ thin film.

ture. During the deposition the substrates were placed on a heater block. The temperature of the block was fixed at 650 °C but according to a pyrometer measurement the surface of the substrate was about 150 °C lower. Pure oxygen, flowing through the chamber at a pressure of 3 mbars, was used as a discharge gas. After the deposition the chamber was immediately vented with oxygen to a pressure of 800 mbars and then allowed to cool down.

III. RESULTS

In x-ray θ-2θ scans only the (001) peaks of both the $SrTiO_3$ substrate and the $SrRuO_3$ thin film were detected. An out of plane pseudocubic lattice constant of 3.957±0.002 Å was found using Rietveld analysis. The periodic intensity oscillations observed at the shoulders of the $SrRuO_3$ (002) x-ray peak [Fig. 1(a)], as a result of reflection at the substrate-film interface, indicate that the interface is sharp and free of intermixing. The thickness derived from their periods is in a good agreement with RBS simulations, and the out of plane lattice constant exactly fits the Rietveld analysis. Typical ω scans of the (002) peak [Fig. 1(b)] show Gaussian-like rocking curves with a FWHM of 0.05°–0.06° (typical FWHM of $SrTiO_3$ substrate is 0.03°). At the ϕ scan of $SrRuO_3$ (221) reflection, measured for 100 nm thick film, four peaks separated by 90° from each other were observed. This result, as shown before in PLD experiments,[27] indicates the coexistence of two orthorhombic $SrRuO_3$ domains with [110] axis normal to the substrate and two in-plane epitaxial arrangements of $SrRuO_3[001] \| SrTiO_3[010]$ and $SrRuO_3[001] \| SrTiO_3[100]$.

The $SrRuO_3$ thin films grown by high pressure sputtering under similar conditions have been used since a long time in multilayer deposition processes and their high quality were confirmed by transmission electron microscopy measurements.[34]

The RBS measurement for a 36 nm thick film (1.4 MeV He^+) shows a minimum ratio (χ_{min}) of the backscattering yield of about 2.2%. The stoichiometry of the films was difficult to determine, however, a simulation gives the best fit to the obtained data for a Ru/Sr ratio=0.84 (Fig. 2).
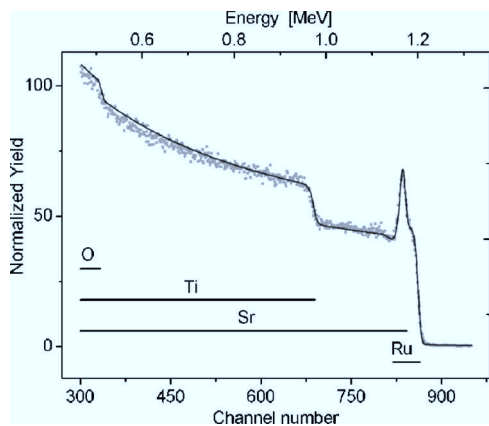
FIG. 2. RBS spectrum of 36 nm thick $SrRuO_3$ film (points) and the best simulation obtained with a Ru/Sr ratio=0.84 (line).

FIG. 4. ToF SIMS depth profile on 50×50 μm^2 area.

The ToF SIMS lateral scans, performed on $SrRuO_3$ thin film areas from 100×100 to 10×10 μm^2 did not reveal any regions of different stoichiometry (Fig. 3). With a resolution of about 300×300 nm^2, the thin film's chemical composition seems to be laterally homogeneous. The ToF SIMS depth profile (Fig. 4) for an area of 50×50 μm^2 shows that the stoichiometry of the film is constant, except for the interface region, where the Sr content is much larger. It suggests that at least one additional SrO layer is present in the standard alternating $SrO-RuO_2$ layer structure, and therefore the occurrence of Ruddlesden-Popper phases. Similar planar defects, recognized as a double SrO layer, were discovered by Jia *et al.*[35] at the $BaTiO_3/SrRuO_3$ interface, formed at the temperature of 800 °C and oxygen pressure of 2×10^{-3} mbar. Another case of a broadened interface on unknown composition between $SrRuO_3$ thin film and $SrTiO_3$ substrate was observed by Lee *et al.*[36] Samples were high quality thin films deposited by PLD at 700 °C and oxygen pressure of 0.13 mbar.

A typical atomic force microscopy (AFM) scan [Fig. 5(a)] shows a very smooth surface of the as-made thin film reflecting substrate steps and similar roughness of a rms value, typically lower than 0.2 nm on areas of 8×8 and 2×2 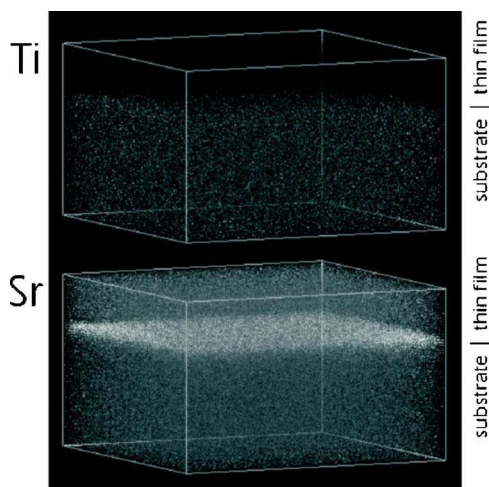μm^2. The film growth is clearly a combination of step flow growth of terraces along the [100] and the [010] substrate axes and two-dimensional nucleation of separate islands at the terraces. This means that the front area of every step consists of small islands of diameter of tens of nanometers, which coalesce in the middle area of the step and form a flat uniform surface at the area where the next step starts being formed.

Smaller scale local conductivity AFM (LC-AFM) and scanning tunneling microscopy (STM) pictures [Figs. 5(b) and 5(c)] revealed a large number of small bulges, of diameter of a few nanometers, present on a flat surface of every

FIG. 3. ToF SIMS three-dimensional (3D) spectrum on 20×20 μm^2 area.
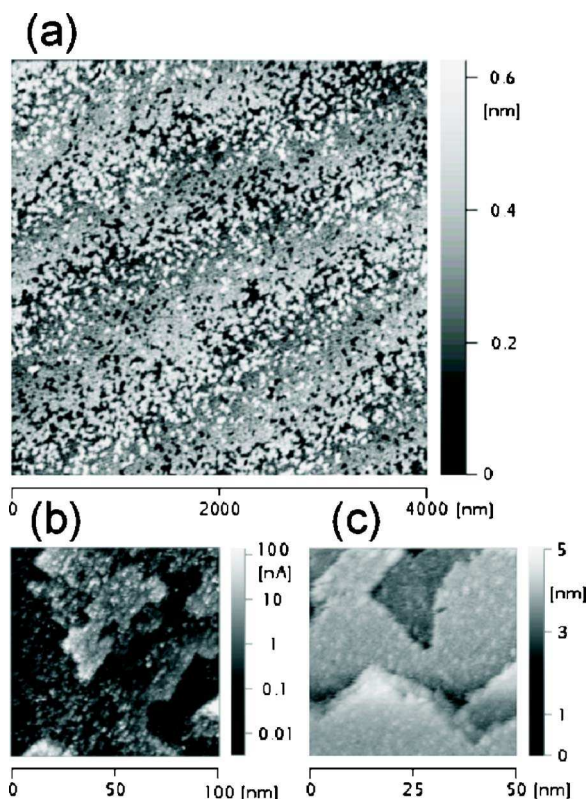

FIG. 5. As-made sample AFM large scan (a), small area LC-AFM scan (log current) (b), and small area STM scan (c).
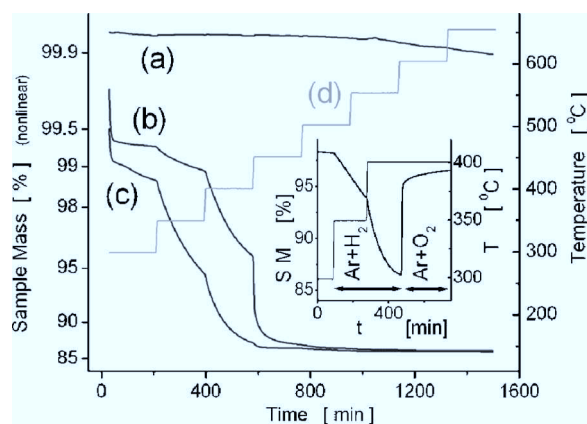
FIG. 6. Thermogravimetry analysis for polycrystalline samples annealed in air (a), 96%Ar+4%H$_2$+40 mbar H$_2$O mixture (b), and 96%Ar+4%H$_2$ mixture (c). The temperature steps during annealing (d). Inset shows reduction of the sample in H$_2$ containing environment and then its oxidation after replacing H$_2$ with O$_2$.

atomic step. Such structures were also observed by other authors and identified as carbohydrate contaminates.[37]

The films show classical metallic behavior[38] in the temperature range of 80–650 K, with a room temperature resistivity, measured using the van der Pauw technique,[39] of about 340 $\mu\Omega$ cm and a slight kink at 153–158 K corresponding to the magnetic phase transition.

We investigated the changes of the surface morphology, crystal lattice parameters, and electronic structure after exposing the SrRuO$_3$ thin films to different environmental conditions.

To determine the temperature range where substantial changes can be expected, first a thermogravimetry analysis, using Netzsch thermobalance type TG439, was performed for polycrystalline samples. A few gram samples were obtained by cutting a ceramic target used for deposition of thin films. θ-2θ x-ray scans showed a full pattern of orthorhombic (*Pnma* space group) SrRuO$_3$ and some low intensity reflections of RuO$_2$. Further chemical analysis gave a Ru/Sr ratio of 1.2, indicating an excess of RuO$_2$ of about 20%. Annealing at 800 °C in 1 bar of a 79%Ar+21%O$_2$ mixture or the same mixture with an addition of 40 mbar H$_2$O did not cause any mass loss of the samples [Fig. 6(a)]. θ-2θ scan of the sample exposed at the pure oxygen atmosphere at the temperature of 800 °C and a pressure of a few millibars remained unchanged.

A large loss of the sample mass occurred rapidly when annealing in 1 bar of a 96%Ar+4%H$_2$ mixture at 400 °C was performed [Fig. 6(b)]. Addition of 40 mbar H$_2$O [Fig. 6(c)] shifts the temperature of this process to about 450 °C but the amount of 12.9% of lost substance is exactly the same. During annealing SrRuO$_3$ decomposed completely following the reaction proposed by Lin *et al.*[40] (SrRuO$_3$+2H$_2$ →Ru+SrO+2H$_2$O). The value of 14.8%, calculated for the full chemical reaction and taking into account 20% RuO$_2$ excess, slightly differed from the experimental value.

Furthermore, in the θ-2θ scan, besides a set of metallic Ru (space group $P6_3/mmc$) peaks, a few unidentified peaks were observed. That may be due to the concurrent formation of complex SrO-H$_2$O compounds, as reported by Halley *et*

al.[41] It is noteworthy that at the temperature as low as 400 °C, when Ar/H$_2$ mixture was replaced by Ar/O$_2$, about 11.2% recovery of sample mass was observed, although no presence of SrRuO$_3$ was found in the θ-2θ scan. This process was identified as ruthenium reoxidation, which was previously reported to occur at this temperature range,[42] for metallic Ru films. The 1.7% difference between the initial and final sample masses may be explained with a not full reoxidation process. The final oxidation state was found to be higher than RuO$_{1.5}$. Some of the missing sample mass may also be volatile SrO. It was found by Shin *et al.*[37] that under high vacuum conditions after heating SrRuO$_3$ up to 500 °C, significant loss of SrO is observed.

According to these results thin films were annealed under different conditions, including short- (1 h) and long- (24 h) term annealings at an oxygen pressure below 10^{-5} mbar and a temperature of about 650 °C, 24 h annealing at 1 atm of air and a temperature of 800 °C, and about 12 h annealing in H$_2$ atmosphere at a pressure of 1 mbar and a temperature of 450 °C. Oxygen partial pressure calculated for hydrogen annealing was lower than 10^{-36} mbar.

Annealing in air at a temperature of 800 °C led to an essential change of the surface topography, measured by AFM. The surface consisted of rectangular regions attaining the width of hundreds of nanometers, ordered in parallel [Fig. 7(b)]. Single regions were flat and free of features and resembled monocrystal grains. rms roughness was about 0.39 nm on an 8×8 μm^2 area. No significant changes in θ-2θ x-ray scans were noticed.

Annealing in vacuum was carried out with the heater temperature varying from 400 to 800 °C in 50 °C steps. At a heater temperature of 800 °C a change in topography was observed [Fig. 7(c)]. The surface was still flat but several precipitates, tens of nanometers in diameter and 5–20 nm high, appeared at the surface, changing the rms roughness to a value of about 0.37 nm on an 8×8 μm^2 area. At this stage the surface temperature, measured by a pyrometer, was about 610 °C.

Long-term vacuum annealing and H$_2$ annealing led to a complete deterioration of the surface [Fig. 7(d)]. In these cases also the SrRuO$_3$ peaks disappeared from θ-2θ x-ray scans, which indicated a decomposition of the bulk structure of the film.

For the as-grown sample and after annealing XPS was carried out *ex situ*, using photons of energy of 1486.6 eV from an Al $K\alpha$ radiation source, a pass energy of 11.2 eV, under the ultrahigh vacuum (UHV) condition of about 10^{-8} mbar. The Sr3*d*, Ru3*p*, O1*s* core lines, as well as the valence band, were measured with a resolution better than 0.1 eV.

Calibration of the position of all the XPS spectra was performed using the Fermi edge as a reference point. In every valence band spectrum, the slope between the occupied and empty electron states was observed at the Fermi level that is at a binding energy of 0 eV.

The spectra of Sr3*d*, O1*s*, and Ru3*p* core lines were taken at an incident beam angle of 50° and then of 10°, where the penetration depth is much lower. For the fitting procedure the spectra measured for one sample at two differ-
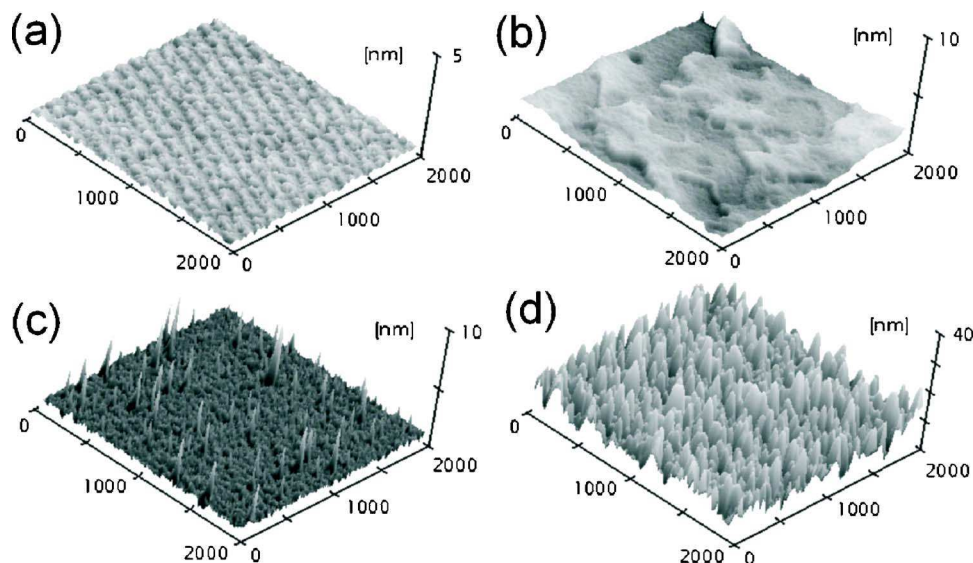
FIG. 7. AFM topography scans for an as-made SrRuO$_3$ thin film (a) and a film annealed in oxygen at 800 °C (b), in vacuum at 600 °C, (c) and in hydrogen at 450 °C (d).

ent angles were initially subtracted (Fig. 8). The difference contained mostly information coming from the deeper layers of the film. It allowed first to distinguish the peaks originating from the atoms involved in the SrRuO$_3$ crystal lattice from the peaks of the surface components, that are atoms bound with physisorbates and chemisorbates at the surface, mainly with carbon oxides and hydroxyls. Enlarged lattice component peaks could be fitted with much higher accuracy, and this way the FWHMs of the lattice component lines were obtained. Then original data were fitted with a number of peaks large enough to match the spectra. The results are presented in a Table I.

In the case of the Sr3d doublet the XPS spectrum of an as-made sample, as well as samples annealed under oxygen-rich and oxygen-deficient conditions, consisted of two significant components. The lattice component doublet position

FIG. 8. Sr3d (I) and O1s (II) core lines of SrRuO$_3$ thin film annealed in oxygen in 800 °C measured by XPS at incident beam angles of 50° (a) and 10° (b), and subtraction (a)−(b) exposing lines from the interior of the film (c). Small bar graphs show relative intensities of the individual components.

and width of lines (0.75 eV) did not change after annealing. The surface component doublet shifted by 0.2 eV to higher binding energy after air annealing and broadened by 0.2 eV after vacuum annealing.

Oxygen O1s spectra in all the above cases also showed the presence of lattice and surface components (Fig. 9) although two surface components were distinguished, which correspond to expected carboxide- and hydroxyl- type contaminations. Oxygen at the energy of about 530.2 eV belongs to SrO−CO$_2$ and at about 531.7 eV to SrO−H$_2$O compounds. The width and position of the very narrow lattice component peak remained unchanged after annealing. Air annealing produced narrowing of the surface component peaks and a shift to higher binding energies. After vacuum annealing, surface components shifted to higher binding energies and hydroxyl component broadened. Therefore annealing in air or vacuum had no influence on the chemical shifts or shapes of the Sr3d or O1s lattice component lines.

In the case of Sr3d and O1s lines, the total area of surface peaks was always larger than the lattice peak area. At the incident beam angle of 10°, the lattice peak intensity was always much lower than the one at an angle of 50°. After both air and vacuum annealings, the amount of the lattice strontium and oxygen became significantly smaller. The largest change was observed for the oxygen spectra after air annealing. Three components were in this case clearly separated, and the carboxide component was much more pronounced. It is worth noticing that the XPS measurements for as-received SrTiO$_3$ substrates show only one sharp Sr3d doublet,[43] suggesting much stronger lattice bonds and thus completely different properties of the surface area.

Using a simple equation given by Cumpson and Seah[44] one can calculate an attenuation length for the electron beam in SrRuO$_3$ and thereby estimate the penetration depth of XPS. For Sr3d electrons with a kinetic energy of 1486.6 −132.1=1354.5 eV, an attenuation length of about 2.2 nm was calculated. Then, in the case of incident beam angle of 50°, 50% of the information comes from the first 5–6 monolayers, while there is still about 10% contribution from below 20 monolayers. Additionally a simple model can be ap-
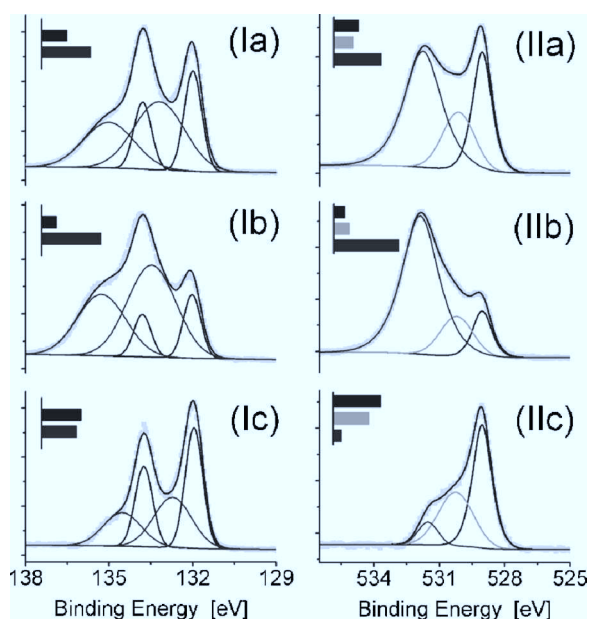
TABLE I. Binding energy, half-width, and mole fraction of the electronic state of the lines fitted to XPS spectra of $SrRuO_3$ as-made thin films, films annealed in air, and films annealed in vacuum.

| | | Sr3d$_{5/2}$ (3d$_{3/2}$) $\Delta=1.8$ eV | | O1s | | | Ru3p$_{3/2}$ (3p$_{1/2}$) $\Delta=22.2$ eV |
		Doublet 1	Doublet 2	Line 1	Line 2	Line 3	Doublet
As-made sample	Energy (eV)	132.1	133.1	529.1	530.1	531.6	464.1
	FWHM (eV)	0.75	2.10	0.95	2.30	2.25	4.55(4.25)
	% mol(50°)(%)	10	11	20		45 (Line2+3)	14
	% mol(10°)(%)	7	14	12		54 (Line2+3)	13
Air annealed sample	Energy (eV)	132.1	133.4	529.0	530.2	531.8	464.3
	FWHM (eV)	0.75	2.10	1.10	1.75	2.10	4.50(3.90)
	% mol(50°)(%)	8	15	19		50 (Line2+3)	9
	% mol(10°)(%)	5	19	8		62 (Line2+3)	6
Vacuum annealed sample	Energy (eV)	132.1	133.2	529.1	530.4	531.8	463.8
	FWHM (eV)	0.75	2.30	1.00	1.90	2.50	4.80(4.40)
	% mol(50°)(%)	9	13	20		45 (Line2+3)	13
	% mol(10°)(%)	5	20	9		57 (Line2+3)	9

plied where the surface component of the thickness d lies on top of the lattice component. As mentioned before the surface component intensity is always higher than 50%, which leads to a minimum thickness of 1 nm.

Having two different incident beam angles, one can show that even this simple model is not accurate. The thickness d of the top layer was calculated using another equation of Cumpson and Seah:[44]

$$d = \lambda \sin \vartheta \ln\left(1 + \frac{I_A/s_A}{I_B/s_B}\right), \tag{1}$$

where λ is an attenuation length, ν is an incident beam angle, and I/s is an intensity divided by a sensitivity factor for an element A from a top layer and B from a bottom layer. When the same element is taken at the top layer and the bottom layer sensitivity factors are equal, the assumption that $\lambda(E_A)=\lambda(E_B)=\lambda$ is satisfied. The results of this calculation are placed in Table II.

For every sample, the thickness of the surface layer calculated at incident beam angle of 50° is about three times larger than at incident beam angle of 10°. Therefore much more of the lattice component was present at low angle measurements than expected from measurements at high angle. The simplest explanation is that either the lattice component is partly uncovered or the surface and lattice components are mixed. In any case one can expect both components to co-exist within five to ten or even more top monolayers.

Every Ru3p XPS spectrum consisted of a single, very broad, and asymmetric doublet (see Ru3p$_{3/2}$ line in Fig. 10). The line was slightly shifted to a higher binding energy after air annealing and to a lower energy after annealing in vacuum. The relative intensity decreased after annealing, regardless of oxygen presence in the ambience. The highest drop was observed at the surface. This lack of ruthenium can be explained with either a different rate of sublimation of the atoms from the surface or a segregation process.[45] Segregation was previously described in the case of $SrTiO_3$ as a dismantling of the SrO layers and a diffusion of material along the extended defects. During oxidation the SrO moved towards the surface and during reduction towards the interior, but some precipitations of SrO appeared on the surface.
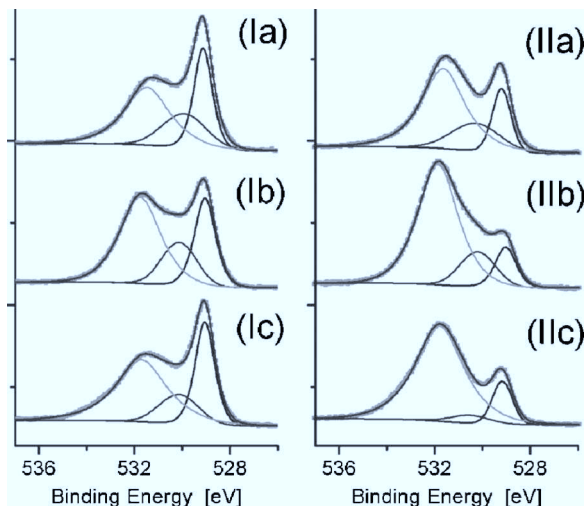

FIG. 9. Oxygen O1s core lines measured by XPS at incident beam angles of 50° (I) and 10° (II) for as-made $SrRuO_3$ thin film (a), sample annealed in oxygen at 800 °C for 24 h (b), and sample annealed in vacuum at 600 °C for 1 h (c).

TABLE II. Calculated thickness (in nm) of the adsorbed contamination layer for $SrRuO_3$ thin films.

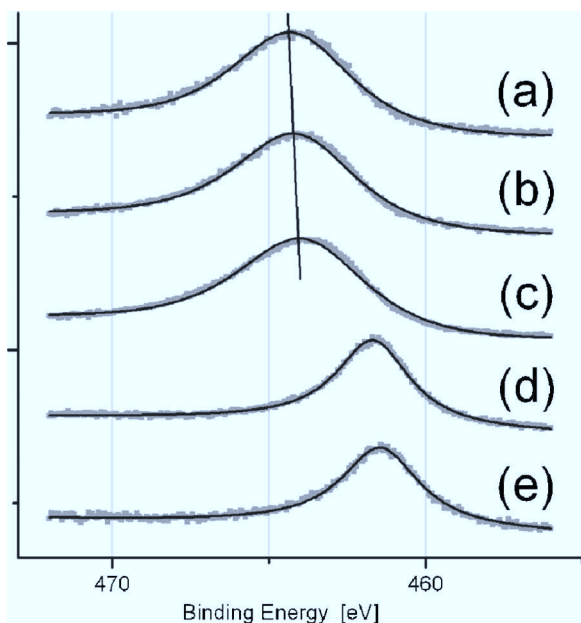| XPS beam angle	XPS core lines	As made	Air annealed	Vacuum annealed
50°	Sr3d	1.54	1.69	1.52
	O1s	1.23	1.83	1.45
10°	Sr3d	0.50	0.63	0.59
	O1s	0.41	0.62	0.59

FIG. 10. Ru$3p_{3/2}$ core lines measured by XPS for sample annealed in air at 800 °C for 24 h (a), as-made SrRuO$_3$ thin film (b), sample annealed in vacuum at 600 °C for 1 h (c), in vacuum for 24 h (d), and in hydrogen for 24 h (e).
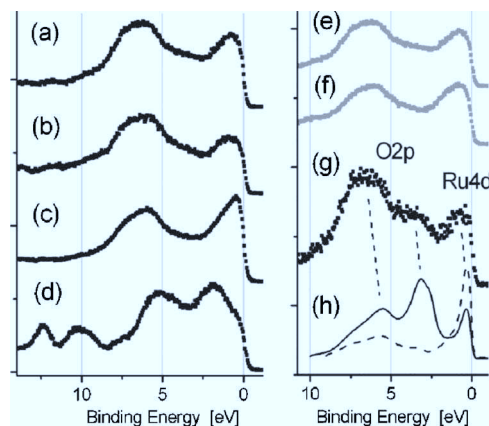

FIG. 11. Valence band spectra measured by XPS ($h\nu=1486.6$ eV) for as-made SrRuO$_3$ thin film (a), sample annealed in oxygen at 800 °C for 24 h (b), annealed in vacuum at 600 °C for 1 h (c), and annealed in hydrogen at 450 °C for 24 h (d). Valence band for as-made sample measured at incidence beam angles of 50° (e) and 10° (f) and (e)−(f) subtraction (g) exposing valence band of the interior of the thin film. Valence band structure calculation (h) of O2p (solid) and Ru4d (dashed) in SrRuO$_3$ (Ref. 48).

In the case of SrRuO$_3$ both oxidation and reduction led to SrO enrichment of the surface region, which suggests that segregation is not dominant.

An unexpectedly large FWHM of the Ru$3p_{3/2}$ line, which in every case exceeded 4.5 eV, is a clear indication that the surface of an as-made SrRuO$_3$ film contains Ru atoms that are not fully oxidized but have mixed oxidation states ranging from Ru^{4+} to Ru^0 (metallic). This situation does not seem to change in the bulk of the film because hardly any change in spectra measured at different incident angles is observed. Only in the case of long-term annealing in the oxygen-scarce environment does the line FWHM decrease by more than 1.6 eV and the binding energy was about 2.5 eV lower (461.6 eV). This is a strong indication that the majority of Ru ions underwent a reduction to the metallic state. Such conclusion is supported by the fact that after a reduction by long-term pure H$_2$ annealing, the Ru$3p_{3/2}$ peak had exactly the same parameters. Simultaneously the lattice part disappeared completely from the Sr3d spectrum in both cases. Similar ruthenium oxidation and reduction processes were presented before by Hartmann *et al.*,[42] for metallic Ru thin films annealed in air, and Ohara *et al.*,[46] for Sr(Ti$_{1-x}$Ru$_x$)O$_3$ thin films annealed in hydrogen. The presented Ru3d spectra always consisted of a low binding energy line related to metallic ruthenium and one or more lines, shifted by 1–2.5 eV to higher binding energies, related to oxidized ruthenium. During air annealing of metallic ruthenium, the line related to metal decreased, while the oxidized ruthenium line became larger and shifted to higher binding energies, which indicates the oxidation process.[43] Both metal and oxide lines were very narrow which may indicate the existence of only Ru^0 and Ru^{4+} states. Annealing of Sr(Ti$_{1-x}$Ru$_x$)O$_3$ in hydrogen caused the oxide line to shift to lower binding energies and finally to vanish, while the

metal line appeared and grew in size.[46] In this case a reduction clearly took place with the presence of intermediate oxidation states.

The general stoichiometry of a surface region derived from XPS spectra, taken at an angle of 50°, for the as-grown thin film was Sr:Ru:O$=1:0.7:3.1$. After a long-term oxygen-rich annealing, stoichiometry observed at the same angle changes to Sr:Ru:O$=1:0.4:3.1$ and short vacuum annealing led to Sr:Ru:O$=1:0.6:2.9$. Longer vacuum treatment, as well as annealing in a H$_2$ containing ambience, led to complete reduction of ruthenium oxide, the disappearance of the Sr3d lattice peaks, and broadening and the intensity decrease of the O1s lattice peaks in the XPS spectrum, as mentioned before. Stoichiometry in both cases was Sr:Ru:O$=1:0.3:2.8$.

The results above are consistent with XPS spectra obtained by Shin *et al.*[37] for PLD thin films. The structure of their Sr3d, O1s, and Ru$3p_{3/2}$ spectra as well as the ratio between the surface and the lattice part were similar, even if the components were broader and not so clearly separated. *In situ* annealing in vacuum shifted the Ru3p peak to lower binding energies and lowered the total O/Sr intensity ratio. Both lattice and surface components were still present. The shift at the annealing temperatures of 600 and 700 °C was larger than 1 eV, while our 30 min annealing at 650 °C caused the shift of only about 0.3 eV. Our longer annealing at the same temperature revealed that the process advanced in time and a final shift of the line was about 2.5 eV. The main difference reported was the Ru/Sr intensity ratio, which was constant during *in situ* vacuum annealing. The starting value of 0.4 was, however, much lower than our ratio of 0.7 and very close to the lowest value obtained by us of 0.3.

The valence bands (Fig. 11) of our SrRuO$_3$ thin films were similar to those presented for polycrystalline samples[47] except that a slope at the Fermi edge was much steeper. Two main features appear in the spectra at binding energies of about 0.8 and 6.4 eV, respectively. Subtraction of the spec-
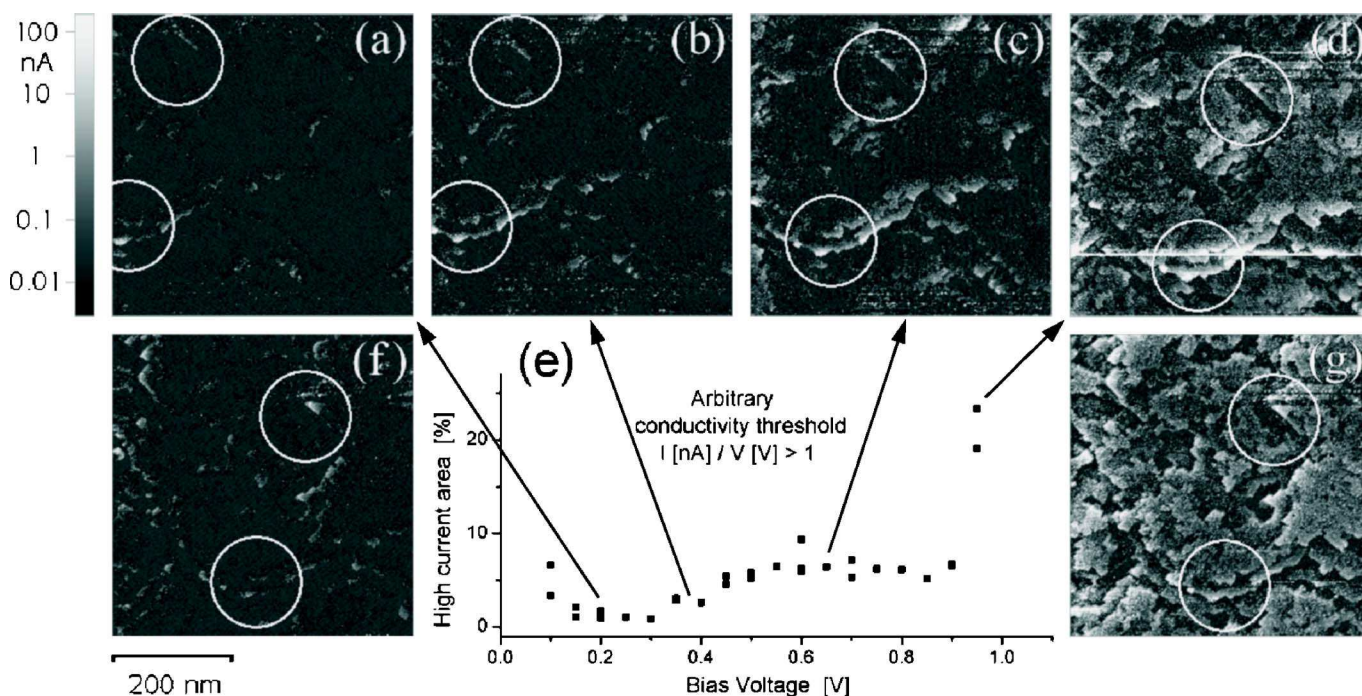
FIG. 12. LC-AFM current images (log scale) taken at increasing bias voltage of 0.3 V (a), 0.4 V (b), 0.6 V (c), and 0.95 V (d). Two features are marked with white circles. Graph (e) shows the area of high conductivity (exceeding arbitrarily defined threshold). Images (f) and (g), taken at 0.2 and 0.95 V, respectively, show surface changes after about 30 scans.

tra, taken at incident beam angles of 50° and 10°, revealed another feature at about 3.4 eV. Comparison with a partial valence band structure calculation of both Ru4d and O2p states,[48] allowed the assumption that the feature close to the Fermi level is derived mainly from Ru4d electrons, while O2p maxima lie at the higher energies. After annealing under oxygen-deficient conditions the Ru4d part increased. Finally, for the samples in which mainly metallic Ru remained, the valence band structure changed completely. The intensity of the Ru4d part of the spectra significantly decreased or it moved to a higher binding energy range. O2p features were likely shifted closer to the Fermi level.

LC-AFM and STM measurements were performed to provide some detailed information about the SrRuO3 thin film surface topography and morphology, as well as to investigate its changes, produced by low energy electron bombardment.

The LC-AFM scans were taken with a bias voltage varying from 0.1 to 0.95 V, with steps of 0.05 V, at the scanned area of 500×500 nm². Regardless of applied bias voltage, the observed surface always consisted of areas of different conductivities. At low voltages, up to 0.3 V, most of the surface remained with very low conductivity [Fig. 12(a)] and no details could be distinguished, except for a few features of very good conductivity. With increasing voltage more of the surface was becoming highly conductive and this process seemed to obey certain threshold voltages. Clearly at the bias voltages of 0.4 and 0.95 V rapid changes in the ratio between low and high conductivity areas were observed [Figs. 12(b)–12(d)]. To estimate these changes quantitatively, arbitrary resistance value, dividing highly conductive and low conductive areas, was taken at $I/U = 1$ nA/V. The results of calculation are presented in Fig. 12(e). After about 30 scans

the bias voltage was decreased and again most of the surface became lowly conductive, according to the previously described voltage thresholds [Fig. 12(f)], although some changes were noticeable in the high conductivity areas. To show these changes two features were marked by circles (Fig. 12). Highly conductive areas were usually the edges of the steps of atomic layers, probably due to the smallest quantity of the surface contaminations. The lower marked feature was clearly such an edge. After several scans it became much less perceptible, which may be an indication of a partial decomposition. At the same time the upper feature became much more pronounced. Several I-V curves, taken at high and low conductivity areas, showed completely different characters (Fig. 13). Typical curves revealed a tunneling character of charge transport [Figs. 13(a) and 13(b)], although conductivity was up to 10^3 times different. Occasionally, after several scans with a bias voltage of about 1 V, metallic characteristics could be obtained [Fig. 13(c)]. The highest and lowest measured conductivities differed by about 10^5 times. The process of a transition from a low to a high conductivity state can be explained by electrically stimulated partial chemical decomposition of the adsorbed layer at first, but with increasing voltage also the decomposition of the first monolayers of the SrRuO3 lattice. When a bias voltage of about −3 V (grounded tip) was used, holes of few nanometers in depth could be obtained. Unfortunately the electrochemical reaction destroyed the conductive coating of AFM tip as well.

The STM scans, taken in the constant current mode, showed the surface to be conductive at the whole area, regardless of an applied bias voltage or a fixed tunneling current, in the ranges of 0.005–1 V and 0.015–5 nA, respectively. Results of measurements in air were similar to those
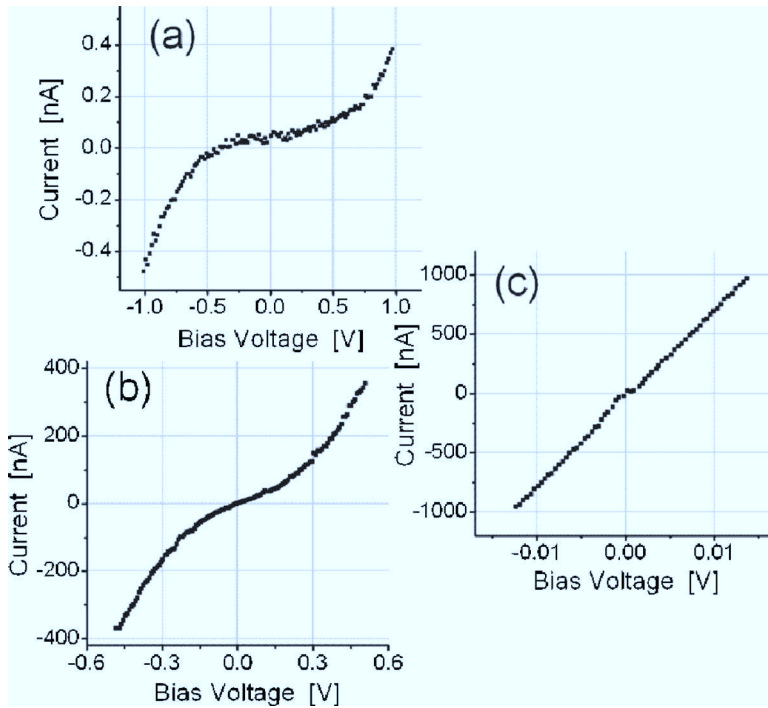
FIG. 13. Typical *I-V* characteristics measured with LC-AFM taken at a low conductivity region (a) and two different types of high conductivity regions [b and c].

obtained under UHV conditions. Using a bias voltage of 30 mV (grounded tip) and a tunneling current of 80 pA on a scanned area of $1 \times 1 \ \mu m^2$, under high vacuum conditions, a sequence of pictures was obtained (Fig. 14). Several 20–100 nm long structures were discovered on a flat surface with visible atomic steps. The material was easily formed below the tip during tunneling. Some parts became larger or smaller and finally disappeared during the process of scanning, indicating a possible mass transport or decomposition. After every transfer above the feature the tip left a tens of nanometer long trace, recorded on the picture. It meant that the structure of this material was rather fragile. The height of about 10 nm excluded the possibility that the observed features consisted of an adsorbed water monolayer. Most likely some $SrO-H_2O$ compounds were detected. The idea that cations at the surface of the thin film may react with water, forming hydroxides, which readily decompose in the electric field, was proposed before. It is possible to remove the $YBa_2Cu_3O_{7-\delta}$ thin films locally using a STM tip and a bias voltage of 1.5 V.[49] In the case of the $SrTiO_3$ thin films, ridges of several nanometer high were formed using a conductive AFM tip and a negative bias voltage in the range of

10–30 V.[50] In both cases transport of a large amount of material is thought to be possible due to the formation and decomposition of $Ba(OH)_2$ and $Sr(OH)_2$.

At first glance the difference between STM and LC-AFM results is surprising. Using STM it is possible to obtain any tunneling current in the range of 100–1000 pA in every scanned surface point, applying a voltage lower than 0.1 V. With LC-AFM and a voltage lower than 1 V there exist large surface areas where obtained current is below the measurement limit that is lower than 10 pA. To explain it one has to focus on a difference of geometry of the measurement. A LC-AFM conductive tip is in contact with a material, which is the conductive $SrRuO_3$ thin film, mixed at the surface region with nonconductive contaminations. When the tip touches an adsorbate layer almost all the potential drops across this layer.[51] Polarized dielectric forms a large potential barrier for the electrons. A STM conductive tip is separated from the material by a vacuum or air gap. In this case most of the potential drops across the gap and a contamination layer is much less polarized which makes the potential barrier lower. Also the electrons approaching the surface have a relatively high kinetic energy. It makes an electron transport
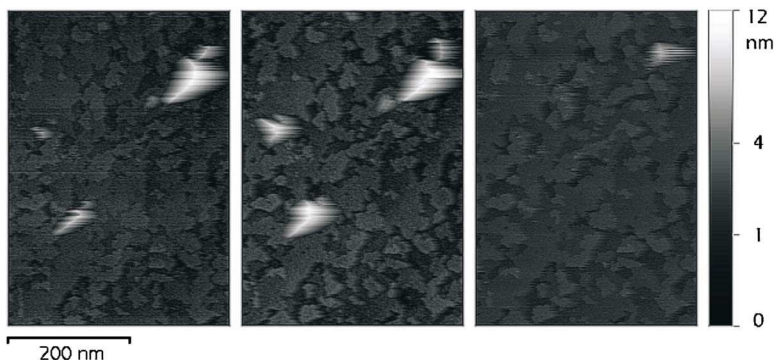

FIG. 14. STM pictures, taken at the area of $1 \times 1 \ \mu m^2$, revealing concentrated groups of adsorbates on the surface of the thin film.

in the case of STM much easier and weakly dependent on the thickness of a contamination layer, while for LC-AFM at a certain applied voltage only these regions are accessible which are uncovered or have a contamination layer thin enough to allow tunneling.

IV. CONCLUSIONS

Standard epitaxial $SrRuO_3$ thin films were prepared using high pressure sputtering. While all the quality parameters commonly used to describe the quality of the film, such as lattice constants, rocking curve FWHM, AFM roughness, or resistivity, showed values within the best possible limits, stoichiometry inhomogeneities were proven to exist at the surface region and interface.

There existed a significant excess of SrO at the surface layer of a reference sample. The value of Ru/Sr ratio measured by XPS at the incident beam angle of 50° was 0.7. Both oxidation and reduction led to a further decrease of this ratio, most likely due to ruthenium (RuO_x) loss. Long oxidation led to a value of 0.4 and reduction in vacuum or hydrogen to a final value of 0.3.

XRD measurements did not reveal any changes of the crystal structure of the film neither after a long treatment in air nor a short-term vacuum annealing. A $SrRuO_3$ pattern disappeared, however, after longer vacuum treatment.

Both air and vacuum annealings led to a deterioration of the surface topography and morphology. During oxidation the $SrRuO_3$ structure tended to form an ordered structure consisting of rectangular flat grains at the surface, while reduction led to the appearance of numerous precipitations on the flat surface of the film first and finally to a complete decomposition of the $SrRuO_3$ structure.

The XPS O1s and Sr3d core spectra consisted of lattice and adsorbed surface compounds. The intensity ratios were obtained and the thickness of adsorbed layer estimated to a value of about 1 nm. Ruthenium at the surface was not fully oxidized, as indicated by the very large width of the Ru3p line. An additional excess of SrO, after oxidation or reduction, clearly increased the chemical affinity of the surface. The degree of oxidation of Ru atoms slightly increased after oxidation and decreased after reduction process.

The valence band spectra of a reference thin film as well as after oxidation or reduction were only partly consistent with theoretical calculations. Subtraction of the spectra obtained at two different incident beam angles allowed us to remove most of the surface contribution and to show the valence band spectrum of the interior of the film. This spectrum consists of three main features and its shape corresponds very well with the theoretical one.

LC-AFM scans showed lateral regions of different conductivities. The samples were covered with a thick and nonuniform layer of nonconductive adsorbates. Electrical contacts form as a result of an electrochemical reaction at the least contaminated areas. If the contact is made on a small area a threshold voltage is needed to overcome an insulating barrier. Electrochemical decomposition of the $SrO-H_2O$ compounds was very easy even with a very small applied voltage, as shown in the STM figures. With an applied voltage of about 3 V, further decomposition of $SrO-CO_2$ structures simultaneously with the top $SrO-RuO_2$ layers was possible.

[1] P. Lu, F. Chu, Q. X. Jia, and T. E. Mitchell, J. Mater. Res. **13**, 2302 (1998).
[2] X. D. Wu, S. R. Foltyn, R. C. Dye, Y. Coulter, and R. E. Muenchausen, Appl. Phys. Lett. **62**, 2434 (1993).
[3] A. P. Mackenzie, J. W. Reiner, A. W. Tyler, L. M. Galvin, S. R. Julian, M. R. Beasley, T. H. Geballe, and A. Kapitulnik, Phys. Rev. B **58**, R13318 (1998).
[4] S. C. Gausepohl, M. Lee, R. A. Rao, and C. B. Eom, Phys. Rev. B **54**, 8996 (1996).
[5] R. A. Rao, D. B. Kacedon, and C. B. Eom, J. Appl. Phys. **83**, 6995 (1998).
[6] M. Wohlfahrt-Mehrens, J. Schenk, P. M. Wilde, E. Abdelmula, P. Axmann, and J. Garche, J. Power Sources **105**, 182 (2002).
[7] G. N. Banerjee, R. N. Bhowmik, and R. Ranganathan, J. Phys.: Condens. Matter **13**, 9481 (2001).
[8] C. Bansal, H. Kawanaka, R. Takahashi, and Y. Nishihara, J. Alloys Compd. **360**, 47 (2003).
[9] C. S. Alexander, G. Cao, S. McCall, and J. E. Crow, J. Appl. Phys. **85**, 6223 (1999).
[10] H.-M. Christen, L. A. Boatner, J. D. Budai, M. F. Chisholm, L. A. Gea, D. P. Norton, C. Gerber, and M. Urbanik, Appl. Phys. Lett. **70**, 2147 (1997).
[11] M. Hiratani, C. Okazaki, K. Imagawa, and K. Takagi, Jpn. J. Appl. Phys., Part 1 **35**, 6212 (1996).
[12] S. H. Oh and C. G. Park, J. Appl. Phys. **95**, 4691 (2004).
[13] L. Miéville, T. H. Geballe, L. Antognazza, and K. Char, Appl. Phys. Lett. **70**, 126 (1997).
[14] P. Khalifah, I. Ohkubo, H. M. Christen, and D. G. Mandrus, Phys. Rev. B **70**, 134426 (2004).
[15] I. Stolichnov, A. Tagantsev, N. Setter, J. S. Cross, and M. Tsukada, Appl. Phys. Lett. **75**, 1790 (1999).
[16] M. Hrovat, S. Bernik, J. Holc, T. Padeznik, and M. Kosec, J. Mater. Sci. **35**, 1725 (2000).
[17] R. Domel, C. L. Jia, C. Copetti, G. Ockenfuss, and A. I. Braginski, Supercond. Sci. Technol. **7**, 277 (1994).
[18] T. Yoshimura and S. Trolier-McKinstry, Appl. Phys. Lett. **81**, 2065 (2002).
[19] C. H. Ahn *et al.*, Appl. Phys. Lett. **70**, 206 (1997).
[20] C. L. Chen *et al.*, Appl. Phys. Lett. **71**, 1047 (1997).
[21] Y. L. Qin, C. L. Jia, K. Urban, J. H. Hao, and X. X. Xi, J. Cryst. Growth **252**, 279 (2003).
[22] S. H. Oh and C. G. Park, Philos. Mag. **83**, 1307 (2003).
[23] K. Szot, W. Speier, J. Herion, and Ch. Freiburg, Appl. Phys. A: Mater. Sci. Process. **64**, 55 (1997).
[24] D. Halley, C. Rossel, D. Widmer, H. Wolf, and S. Gariglio, Mater. Sci. Eng., B **109**, 113 (2004).
[25] X. Fang and T. Kobayashi, J. Appl. Phys. **90**, 162 (2001).
[26] S. S. Kim, T. S. Kang, and J. H. Je, J. Appl. Phys. **90**, 4407 (2001).
[27] Q. Gan, R. A. Rao, and C. B. Eom, Appl. Phys. Lett. **70**, 1962 (1997).
[28] Z. R. Dai, S. Y. Son, B. S. Kim, D. K. Choi, and F. S. Ohuchi, Mater. Res. Bull. **34**, 933 (1999).
[29] S. Ohashi, M. Lippmaa, N. Nakagawa, H. Nagasawa, H. Koinuma, and M. Kawasaki, Rev. Sci. Instrum. **70**, 178 (1999).
[30] M. A. López de la Torre, Z. Sefrioui, D. Arias, M. Varela, J. E. Villegas, C. Ballesteros, C. León, and J. Santamaría, Phys. Rev. B **63**, 052403 (2001).
[31] N. Okuda, K. Saito, and H. Funakubo, Jpn. J. Appl. Phys., Part 1 **39**, 572 (2000).
[32] J. P. Mercurio, J. H. Yi, M. Manier, and P. Thomas, J. Alloys Compd. **308**, 77 (2000).
[33] E. Vasco, R. Dittmann, S. Karthäuser, and R. Waser, Appl. Phys. A: Mater. Sci. Process. **79**, 1461 (2004).
[34] C. L. Jia, J. Rodríguez Contreras, U. Poppe, H. Kohlstedt, R. Waser, and K. Urban, J. Appl. Phys. **92**, 101 (2002).

[35] C. L. Jia, J. Rodríguez Contreras, J. Schubert, M. Lentzen, U. Poppe, H. Kohlstedt, K. Urban, and R. Waser, J. Cryst. Growth **247**, 381 (2003).

[36] H. N. Lee, H. M. Christen, M. F. Chisholm, C. M. Rouleau, and D. H. Lowndes, Appl. Phys. Lett. **84**, 4107 (2004).

[37] J. Shin, S. V. Kalinin, H. N. Lee, H. M. Christen, R. G. Moore, E. W. Plummer, and A. P. Baddorf, Surf. Sci. **581**, 118 (2005).

[38] L. Klein, J. S. Dodge, C. H. Ahn, J. W. Reiner, L. Mieville, T. H. Geballe, M. R. Beasley, and A. Kapitulnik, J. Phys.: Condens. Matter **8**, 10111 (1996).

[39] L. J. van der Pauw, Philips Tech. Rev. **20**, 220 (1958).

[40] J. Lin, K. Natori, Y. Fukuzumi, M. Izuha, K. Tsunoda, K. Eguchi, K. Hieda, and D. Matsunaga, Appl. Phys. Lett. **76**, 2430 (2000).

[41] D. Halley, C. Rossel, D. Widmer, H. Wolf, and S. Gariglio, Mater. Sci. Eng., B **109**, 113 (2004).

[42] A. J. Hartmann, M. Neilson, R. N. Lamb, K. Watanabe, and J. F. Scott, Appl. Phys. A: Mater. Sci. Process. **70**, 239 (2000).

[43] K. Szot, W. Speier, U. Breuer, R. Meyer, J. Szade, and R. Waser, Surf. Sci. **460**, 112 (2000).

[44] P. J. Cumpson and M. P. Seah, Surf. Interface Anal. **25**, 430 (1997).

[45] Y. Liang and D. Bonnell, J. Am. Ceram. Soc. **78**, 2633 (1995).

[46] R. Ohara, T. Schimizu, K. Sano, M. Yoshiki, and T. Kawakubo, Jpn. J. Appl. Phys., Part 2 **40**, 1384 (2001).

[47] M. V. Rama Rao, V. G. Sathe, D. Sornadurai, B. Panigrahi, and P. Shripathi, J. Phys. Chem. Solids **62**, 797 (2001).

[48] D. Singh, J. Appl. Phys. **79**, 4818 (1996).

[49] G. Bertsche, W. Clauss, F. E. Prins, and D. P. Kern, J. Vac. Sci. Technol. B **16**, 2833 (1998).

[50] L. Pellegrino, I. Pallecchi, D. Marré, E. Bellingeri, and A. S. Siri, Appl. Phys. Lett. **81**, 3849 (2002).

[51] F. Peter, A. Rdriger, R. Dittmann, R. Waser, K. Szot, B. Reichenberg, and K. Prume, Appl. Phys. Lett. **87**, 082901 (2005).